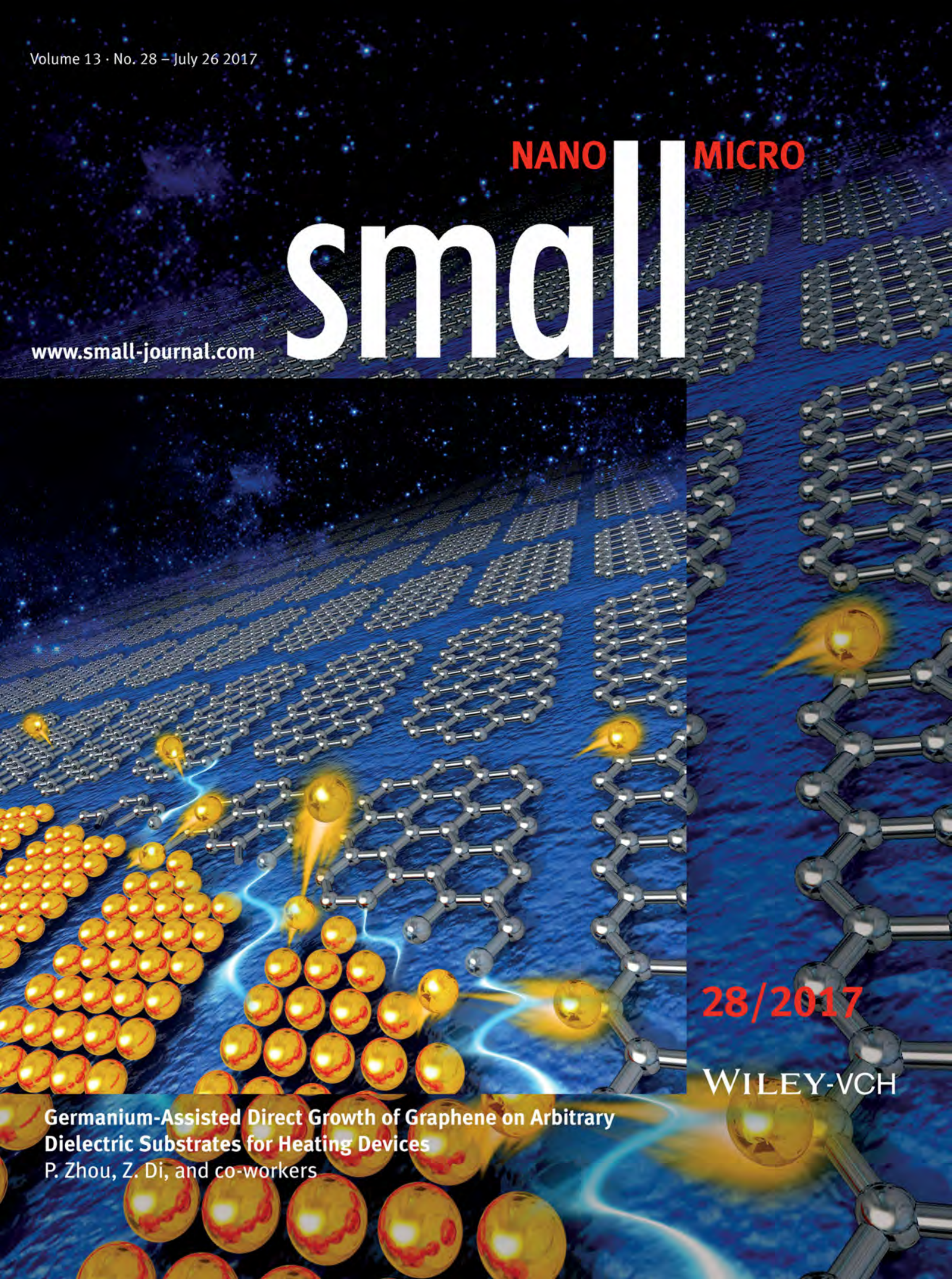

Volume 13 · No. 28 – July 26 2017
NANO
MICRO
small
www.small-journal.com
28/2017
WILEY-VCH
Germanium-Assisted Direct Growth of Graphene on Arbitrary Dielectric Substrates for Heating Devices
P. Zhou, Z. Di, and co-workers

Germanium-Assisted Direct Growth of Graphene on Arbitrary Dielectric Substrates for Heating Devices

Ziwen Wang, Zhongying Xue, Miao Zhang, Yongqiang Wang, Xiaoming Xie, Paul K. Chu, Peng Zhou, Zengfeng Di,* and Xi Wang*

Direct growth of graphene on dielectric substrates is a prerequisite to the development of graphene-based electronic and optoelectronic devices. However, the current graphene synthesis methods on dielectric substrates always involve a metal contamination problem, and the direct production of graphene patterns still remains unattainable and challenging. Herein, a semiconducting, germanium (Ge)-assisted, chemical vapor deposition approach is proposed to produce monolayer graphene directly on arbitrary dielectric substrates. By the prepatterning of a catalytic Ge layer, the graphene with desired pattern can be achieved conveniently and readily. Due to the catalysis of Ge, monolayer graphene is able to form on Ge-covered dielectric substrates including SiO_2/Si, quartz glass, and sapphire substrates. Optimization of the process parameters leads to complete sublimation of the catalytic Ge layer during or immediately after formation of the monolayer graphene, enabling direct deposition of large-area and continuous graphene on dielectric substrates. The large-area, highly conductive graphene synthesized on a transparent dielectric substrate using the proposed approach has exhibited a wide range of applications, including in both defogger and thermochromic displays, as already successfully demonstrated here.

Dr. Z. Wang, Prof. Z. Xue, Prof. M. Zhang, Prof. X. Xie, Prof. Z. Di, Prof. X. Wang
State Key Laboratory of Functional Materials for Informatics
Shanghai Institute of Microsystem and Information Technology
Chinese Academy of Sciences
865 Changning Road, Shanghai 200050, China
E-mail: zfdi@mail.sim.ac.cn

Prof. Y. Wang
Materials Science and Technology Division
Los Alamos National Laboratory
Los Alamos, NM 87545, USA

Prof. P. K. Chu
Department of Physics and Materials Science
City University of Hong Kong
Tat Chee Avenue, Kowloon, Hong Kong 999077, China

Prof. P. Zhou
State Key Laboratory of ASIC and System
School of Microelectronics
Fudan University
Shanghai 200433, China
E-mail: pengzhou@fudan.edu.cn

DOI: 10.1002/smll.201700929

1. Introduction

Graphene, the first stable 2D crystal, is considered to be a basic building block of other important allotropes of carbonic materials.[1] Owing to its high mobility, high conductivity, and superior mechanical properties,[2] graphene has many potential applications, especially in electronic and optoelectronic devices.[3–11] In most applications, high-quality graphene needs to be transferred or directly grown on dielectric substrates. However, transferring the chemical vapor deposition (CVD) graphene films onto dielectric substrates inevitably introduces unintentional contamination, which degrades the physical properties through the formation of defects, impurities, wrinkles, cracks, or even tears.[12–14] Furthermore, in graphene-based device fabrication, transferring specific and extrinsic graphene patterns to the predesigned locations on dielectric substrates gives rise to additional technical challenges. To bypass the transfer process, intense efforts have been made in an attempt to develop CVD approaches to directly grow graphene on dielectric substrates. Ismach et al. reported a pioneer metal-catalyzed transfer-free method,[15] and other modified routes have been proposed by other

 © 2017 Wiley-VCH Verlag GmbH & Co. KGaA, Weinheim

ADVANCED SCIENCE NEWS
www.advancedsciencenews.com

research groups.[16–19] The graphene layers are prepared on a sacrificial metal film, followed by metal dewetting and evaporating at an elevated temperature for extended annealing time. However, metal residues are unavoidable, thus degrading the graphene properties. The successive remote metal catalyzation approach addresses the metal residue issue,[20,21] but the metal contamination problem, which is fatal to semiconductor devices, cannot be solved. Alternatively, the direct metal-catalyst-free growth of graphene on a dielectric substrate, such as Al_2O_3,[22,23] Si_3N_4,[24,25] exfoliated h-BN,[26] MgO,[27] $SrTiO_3$,[28] SiO_2,[29–32] polydimethylsiloxane,[33] and glass,[34,35] shows its advantages in terms of no metal contamination, but the synthesized graphene usually contains substantial defects because of limited catalytic activity of the dielectric materials. Because of insufficient pyrolysis of the precursor gases, the growth process requires high temperature[22] or annealing for a long time.[25] Furthermore, the remote metal catalyzation technique or direct metal-catalyst-free growth method is incapable of producing graphene with the desirable patterns that are essential to graphene-based devices.

Germanium (Ge), which is isoelectronic to Si, has been adopted by the semiconductor industry in strain engineering since the 90-nm technology node in 2003.[36] Since then, Ge has been incorporated into every technology node to build strained Si channels, even in the current state-of-art fin field effect transistor (FinFET) technology.[37] Here, we report metal-free Ge-assisted growth of graphene on various dielectric substrates such as SiO_2/Si, quartz glass, and sapphire. In this technique, patterned graphene can be produced on dielectric substrates easily by prepatterning the Ge film. Graphene formed on transparent dielectric substrates have demonstrated their potential in heating-device applications, including a defogger and thermochromic display, and both devices exhibit excellent performances. Given that Ge has been widely used in every recent semiconductor technology node, we believe that the graphene on dielectric substrates synthesized by the proposed strategy can expedite the practical application of graphene in electronic and optoelectronic devices.

2. Results and Discussion

Figure 1a illustrates the basic concept of Ge-assisted direct growth of graphene on dielectric substrates. The 200-nm-thick Ge layer is deposited on the dielectric substrate by direct-current (DC) magnetron sputtering, and then graphene is produced on the Ge-coated dielectric substrate by CVD for 60–300 min at 900–930 °C (see the Experimental Section for more details).[38] As the temperature is close to the melting point of Ge, the Ge catalyst layer is evaporated

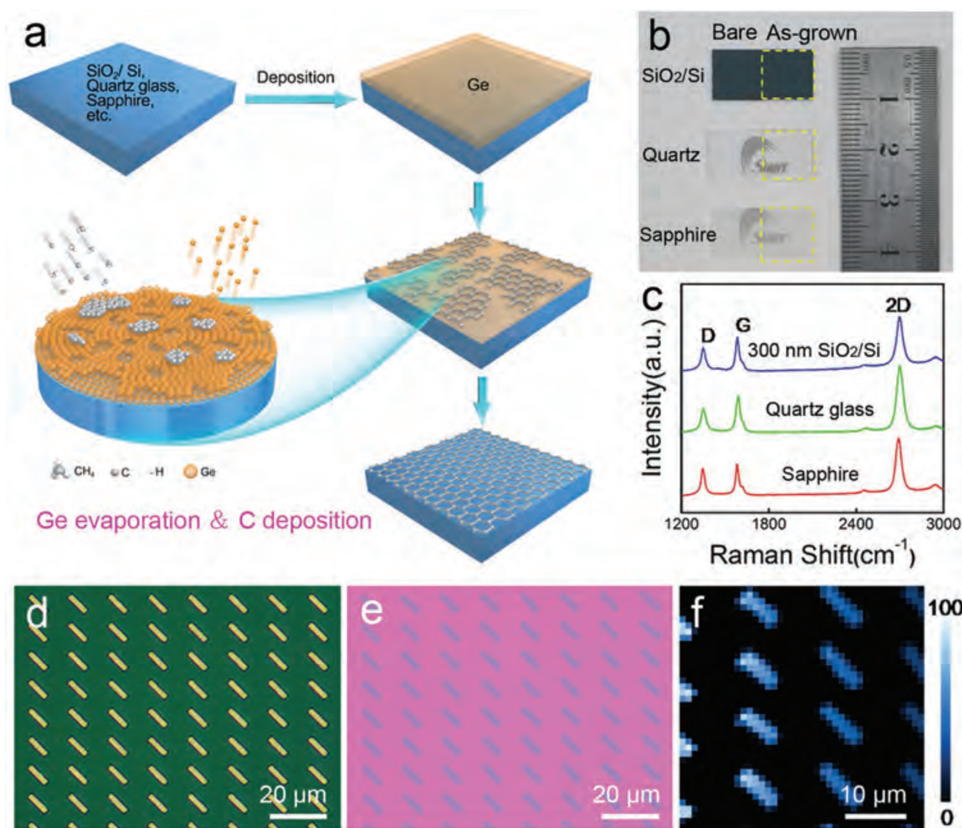

Figure 1. a) Schematic illustration of Ge-assisted direct growth of graphene on arbitrary dielectric substrates. b) Photograph of SiO_2/Si, quartz glass, and sapphire substrates before and after graphene growth. The yellow boxes are drawn to state the regions of interest. c) Raman scattering spectra of the graphene covered SiO_2/Si, quartz glass, and sapphire substrates. d) Optical microscopy image of the prepatterned Ge layer on the SiO_2/Si substrate. e) Optical microscopy image of the graphene pattern on the SiO_2/Si substrate. f) Raman intensity mapping of the 2D peak of the graphene pattern on the SiO_2/Si substrate shown in (e).

 © 2017 Wiley-VCH Verlag GmbH & Co. KGaA, Weinheim

gradually during the graphene growth. By optimizing the conditions, the formation of continuous graphene and the evaporation of the entire Ge layer can be accomplished simultaneously to form graphene on the dielectric substrate directly. Figure 1b displays the images of the pristine and graphene-coated dielectric substrates, including SiO_2/Si, quartz glass, and sapphire, and a uniform color indicates good graphene uniformity. The graphene films on different dielectric substrates are characterized by Raman scattering, as shown in Figure 1c. The characteristic peaks of graphene at D, G, and 2D bands can be observed,[39] but that of the Ge layer is not observed (not shown), indicating the direct growth of graphene on three dielectric substrates with the complete evaporation of the Ge layer. The ratios of the 2D peak to G peak (I_{2D}/I_G) of graphene on SiO_2/Si, quartz glass, and sapphire are 1.43, 1.76, and 1.69, respectively. Furthermore, the 2D peak for each graphene covered dielectric substrate possesses a symmetric shape with one single Lorentzian profile (Figure S1, Supporting Information). Therefore, it is concluded that the synthesized graphene on dielectric substrates is monolayered.[40] The UV–vis transmittance spectra further confirm the synthesis of monolayered graphene, as shown in Figure S2 (Supporting Information).[41] In addition to the large-scale continuous graphene, graphene patterns—the essential building blocks in graphene-based electronic and optoelectronic devices—can be prepared directly by this technique. By prepatterning of the Ge layer (Figure 1d), graphene islands with the same pattern can be grown on the SiO_2/Si substrate, as shown in Figure 1e. The corresponding color-coded intensity mapping of the 2D peak (Figure 1f) suggests that the graphene pattern has good uniformity. Meanwhile, graphene islands with arbitrary patterns can be obtained by our approach, as shown in Figure S3 (Supporting Information).

To elucidate the mechanism of Ge-assisted direct growth of graphene on dielectric substrates, the effects of the growth time and temperature are studied, as shown in **Figures 2** and 3. Scanning electron microscopy (SEM) (Figure 2a1–e1), integrated Raman intensity mapping of the Ge peak (Figure 2a2–e2), and energy-dispersive X-ray spectroscopy mapping (Figure S4 and Table S1, Supporting Information) are performed to monitor the evolution of the Ge layer. Dewetting and evaporation occur as the graphene layer starts to grow. The Ge layer breaks into fragments, but interconnected Ge areas still exist after 60 min. The interconnected Ge areas further evolve into fingerlike structures after 120 min, similar to that observed from Cu films previously.[15] The Ge layer is entirely evaporated after 300 min of CVD growth. Gradual

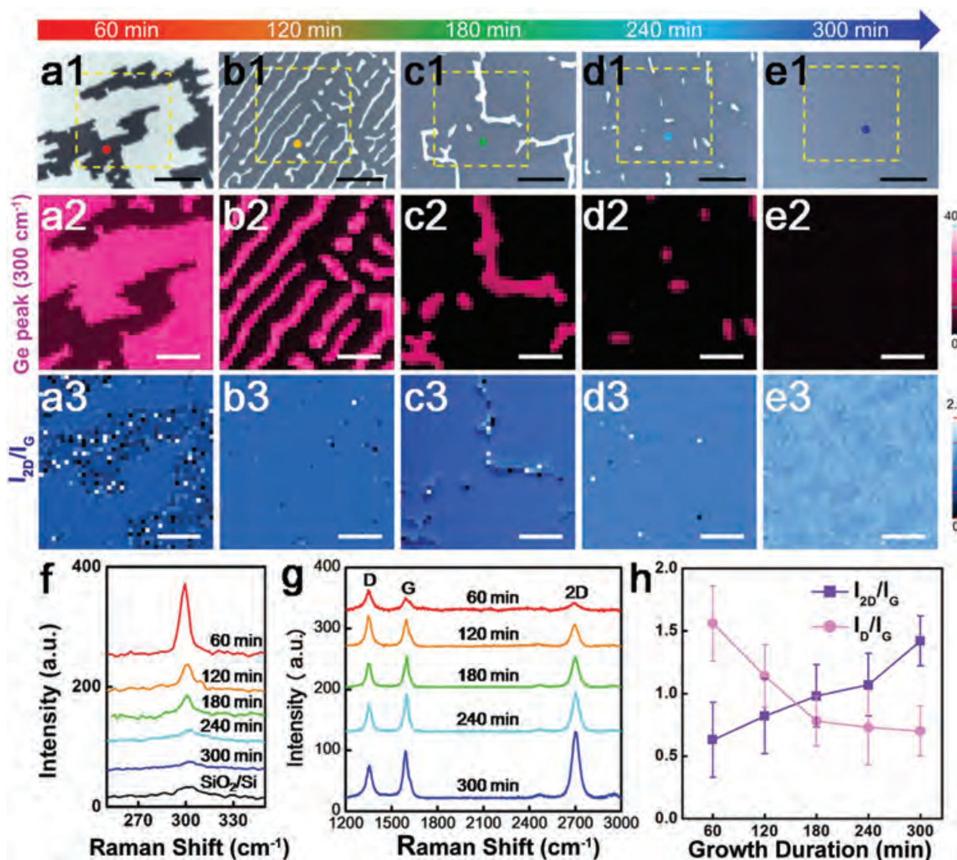

Figure 2. Evolution of Ge evaporation and graphene formation with CVD time. a1–e1) Optical images of graphene grown on SiO_2/Si at 920 °C for different times. Scale bar: 20 µm. a2–e2) Raman mappings of the Ge peak intensity as a function of growth time. The mapped areas are selected in (a1–e1) as denoted by dashed yellow squares. Scale bar: 10 µm. a3–e3) Raman mappings of the I_{2D}/I_G ratio of graphene. Scale bar: 10 µm. f) Raman spectra of Ge for different CVD times at 920 °C. g) Raman spectra of graphene for different CVD times at 920 °C. f) and g) are measured from the color dots marked in (a1–e1). h) Statistical I_{2D}/I_G and I_D/I_G ratios as a function of time, each data point comes from the statistical result of the corresponding Raman mappings.

 © 2017 Wiley-VCH Verlag GmbH & Co. KGaA, Weinheim

ADVANCED SCIENCE NEWS
www.advancedsciencenews.com

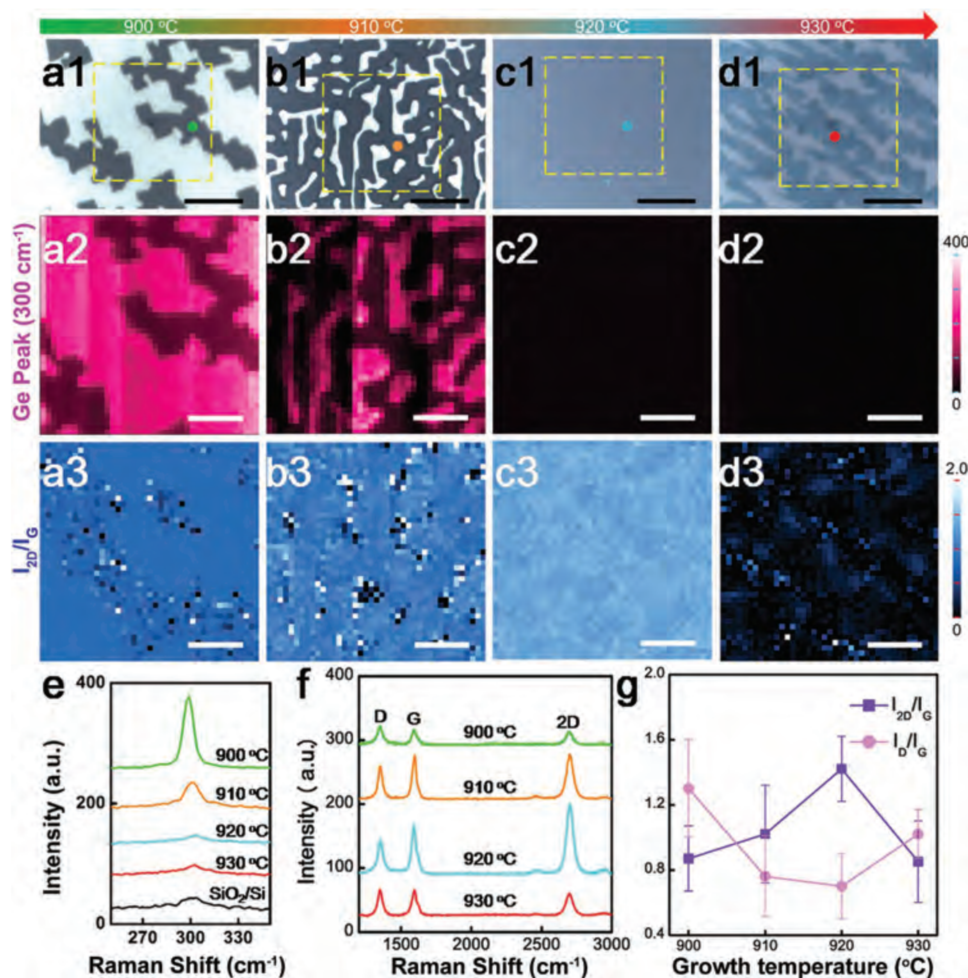

Figure 3. Evolution of Ge evaporation and graphene formation with the CVD temperature. a1–d1) Optical images of graphene grown on SiO_2/Si at different temperatures for 300 min. Scale bar: 20 µm. a2–d2) Raman mappings of the Ge peak intensity as a function of temperature. The mapped areas are selected in (a1–d1) as denoted by dashed yellow squares. Scale bar: 10 µm. a3–d3) Raman mappings of the I_{2D}/I_G ratio of graphene. Scale bar: 10 µm. e) Raman spectra of Ge after graphene growth at different temperatures for 300 min. f) Raman spectra of graphene grown at different temperatures for 300 min. e) and f) are measured from color dots marked in (a1–d1). g) Statistical I_{2D}/I_G and I_D/I_G ratios as a function of temperature, each data point comes from the statistical result of the corresponding Raman mappings.

removal of the Ge layer by evaporation is also confirmed by the Raman scattering spectra (Figure 2f) acquired from the selected areas shown in Figure 2a1–e1. Figure 2f also suggests that even in the regions between the fingerlike structures, there is Ge signal in the initial stage (60–180 min), but the residual Ge evaporates completely after 240 min, as shown by the disappearance of the associated Ge Raman peak at 300.4 cm^{-1}, whereas a new Raman peak corresponding to Si substrate appears at 303 cm^{-1}. The existence of Ge either in the fingerlike structure or beyond the finger area causes strong absorption and scattering of the excitation laser, and therefore, the intensity of the characteristic Raman peaks corresponding to the graphene overlayer is attenuated considerably, as shown in Figure S5 (Supporting Information). In other words, the scanning Raman image of a 2D band of graphene is closely related to the amount of residual Ge (Figure S6, Supporting Information), and only the mapping of I_{2D}/I_G ratio can avoid the influence from Ge residual on SiO_2/Si substrate, thus revealing the distribution of the grown graphene (Figure 2a3–e3). The graphene becomes more uniform as residual Ge evaporates gradually with time. For the growth time less than 300 min, the crystalline quality of graphene is also improved with the prolonged growth time, as suggested by the raw Raman data (Figure 2g) together with the increased I_{2D}/I_G ratio and the decreased I_D/I_G ratio shown in Figure 2h. It should be noted that the crystalline quality of graphene will not significantly change as the growth time is extended for more than 300 min (Figure S7, Supporting Information), indicating that Ge catalyst layer has been evaporated completely and the continuous graphene layer has formed after 300 min.

The effect of temperature on the Ge-assisted direct growth of graphene on dielectric substrates is also carefully investigated, as shown in **Figure 3**. At temperature between 900 and 930 °C, a sufficiently long time of 300 min is used to enable sufficient Ge evaporation and graphene growth. The SEM images (Figure 3a2,b2) and integrated Raman intensity mappings of the Ge peak (Figure 3a3,b3) suggest that evaporation of Ge is retarded at 900–910 °C and a considerable amount of Ge still exists after 300 min. However, the

 © 2017 Wiley-VCH Verlag GmbH & Co. KGaA, Weinheim

evaporation rate of Ge increases at 920–930 °C and the Ge layer is entirely evaporated after 300 min CVD growth. Similar conclusions can be drawn from the raw Raman data in Figure 3e. With regard to the graphene fabricated at 930 °C, the evaporation rate of Ge is too large for the formation of a continuous graphene layer and so only graphene fragments are produced prior to complete evaporation of Ge, as shown in Figure 3d1–d3. With respect to the graphene grown at a temperature lower than 930 °C, the graphene layer with continuous coverage is formed, but the uniformity is better at a higher growth temperature, as shown by Figure 3a3–c3. In addition, the crystalline quality of the synthesized graphene becomes better for relatively high temperatures, as suggested by Raman spectra shown in Figure 3f, besides larger I_{2D}/I_G and smaller of I_D/I_G in Figure 3g. It is concluded that 920 °C is the optimal temperature for the growth of high-quality continuous graphene on dielectric substrates.

Figure 4 shows the detailed structural characterization of the graphene prepared on a SiO_2/Si substrate at 920 °C for 300 min. Prior to graphene growth, the Ge 3d5 peak originates from the Ge layer, and the high-resolution C 1s spectrum (left inset in Figure 4a) only consists of the carbon sp^3-hybridization peak at 285.4 eV arising from natural carbon contamination. After deposition of the continuous graphene layer, the Ge 3d5 peak disappears and the intensity of the C 1s peak increases. The high-resolution C 1s signal (right inset in Figure 4a) indicates that the sp^3-related peak recedes as a clear sharp carbon sp^2-hybridization peak at 284.0 eV emerges, indicative of the formation of the sp^2 network, i.e., graphene. The crystallographic information is provided by transmission electron microscopy (TEM) and selected-area electron diffraction (SAED). The high-resolution TEM (HR-TEM) (Figure 4d) image acquired from the crack edge of the graphene film (Figure 4c) exhibits single layer characteristics. The SAED pattern (Figure 4e) shows multiple sets of spots with hexagonal distributions, indicating the formation of polycrystalline graphene consisting of multiple grains. Figure 4f shows the light intensity of the four spots marked by the dashed box in Figure 4e. The intensity ratio (outermost to innermost) of ≈1:2 suggests the formation of monolayer graphene. A back-gated graphene FET (GFET) device is fabricated to evaluate the transport properties of the monolayer graphene. The schematic structure and typical transfer curve (I_{DS}–V_G) measured at room temperature under ambient conditions are shown in Figure 4b and Figure S8 (Supporting Information), respectively. The transfer curve acquired at V_{DS} of 100 mV shows that both hole and electron conduction can be achieved by gating. The Dirac point of the GFET is at a positive gate voltage of V_G = 11.2 V, suggesting that the graphene is p-doped due to possible water/oxygen adsorption. The extracted field-effect hole and electron mobilities at room temperature are determined to be μ_h = 730 cm^2 V^{-1} s^{-1} and μ_e = 570 cm^2 V^{-1} s^{-1}, respectively, which are comparable to the carrier mobilities of the graphene grown on SiO_2 by catalytic Cu.[42]

To explore potential applications of the continuous conductive graphene on dielectric substrates, heating devices are fabricated using the graphene grown on a quartz glass substrate. Transparent graphene heating devices have been demonstrated in defogging applications, schematically illustrated in **Figure 5**a. When the transparent graphene heater is placed above a beaker containing half a cup of hot water, the surface is quickly covered by fog. As a bias of 20 V is

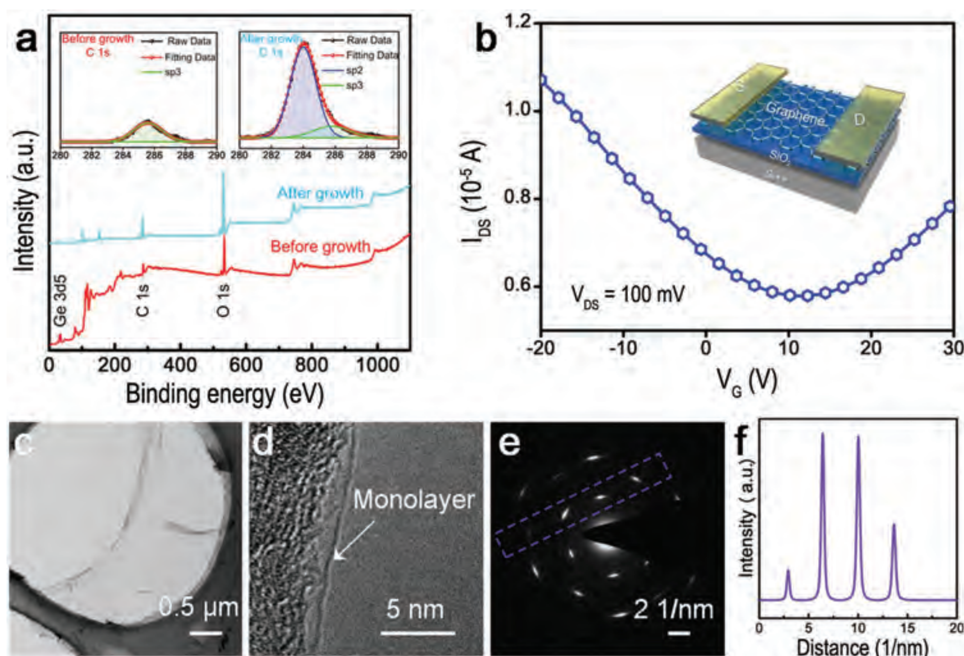

Figure 4. Characterization of monolayer graphene directly grown on SiO_2/Si by Ge-assisted growth. a) XPS analysis of the SiO_2/Si substrate before and after graphene growth. The insets depict the corresponding C 1s peak. b) Transfer characteristics (I_{DS}–V_G) of the graphene transistor at V_{DS} = 100 mV. Inset: Schematic image of the fabricated GFET device. c) Low-magnification TEM image of the graphene transferred onto the copper grid. d) HR-TEM image of the graphene edge. e) SAED pattern of graphene. f) Profiles of diffraction spot intensities along the dashed box in (e).

© 2017 Wiley-VCH Verlag GmbH & Co. KGaA, Weinheim

ADVANCED SCIENCE NEWS
www.advancedsciencenews.com

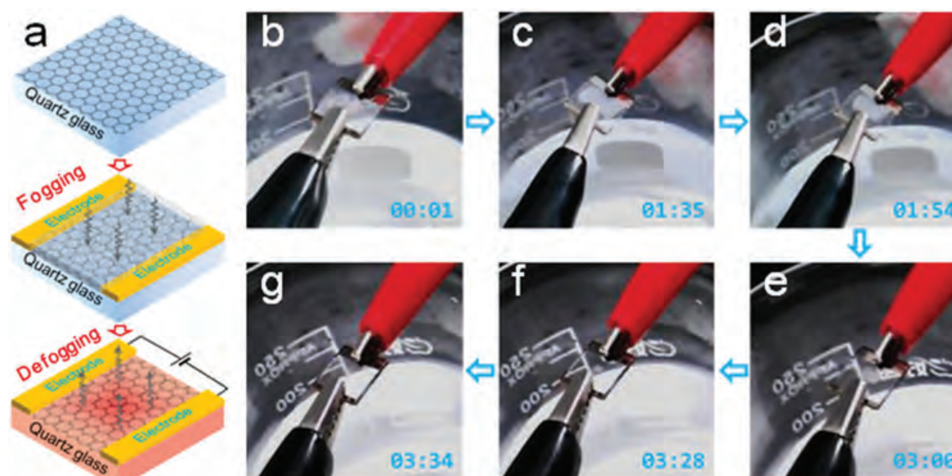

Figure 5. Heating devices fabricated on graphene on quartz glass for defogging application. a) Schematic diagrams showing the fogging and defogging process. b–g) Snapshots of the defogging process at a bias of 20 V.

applied, the defogging process commences. The snapshots shown in Figure 5b–g illustrate the defogging process, which starts from the outer region and extends toward the central region. Finally, the fog disappears completely, revealing good transparency of the graphene heater. Complete defogging shows that the graphene layer on quartz glass is continuous and rather uniform. The real time defogging phenomenon is shown in Figure S9 (Supporting Information).

The transparent graphene heating device can also be used in thermochromic display. A 2D code of "SIMIT" (abbreviation of our institute) is drawn on the heater surface by silk-screen printing using a color reversible thermochromic ink with two color changing stages (purple to blue at 33 °C and blue to gray at 41 °C), as schematically shown in **Figure 6**a. When a small DC bias of 30 V is applied, the purple color changes to blue at 48 s and then gray at 98 s (Figure 6b and Video S1 (Supporting Information)). The transition rate can be enhanced by applying a higher bias at 40 V. As it is increased to 40 V, the first color transition occurs at 26 s and the second one at 53 s, as shown in Figure 6c and Video S2 (Supporting Information). At a certain bias, the time needed to complete the color transition remains same between different cycles, as shown in Figure 6d. However, for graphene grown on insulating solid glasses by catalyst-free atmospheric-pressure chemical vapor deposition approach,[35] it is observed that the color transition time of graphene based thermochromic display device increases gradually during repetitive tests. Therefore, the stability of thermochromic display device in our study is improved, which may be attributed to the improved crystalline quality of graphene due to the catalytic effect of Ge.

3. Conclusion

A metal-free Ge-assisted CVD technique is described to produce single-layer graphene directly on arbitrary dielectric substrates including SiO_2/Si, quartz glass, and sapphire. By

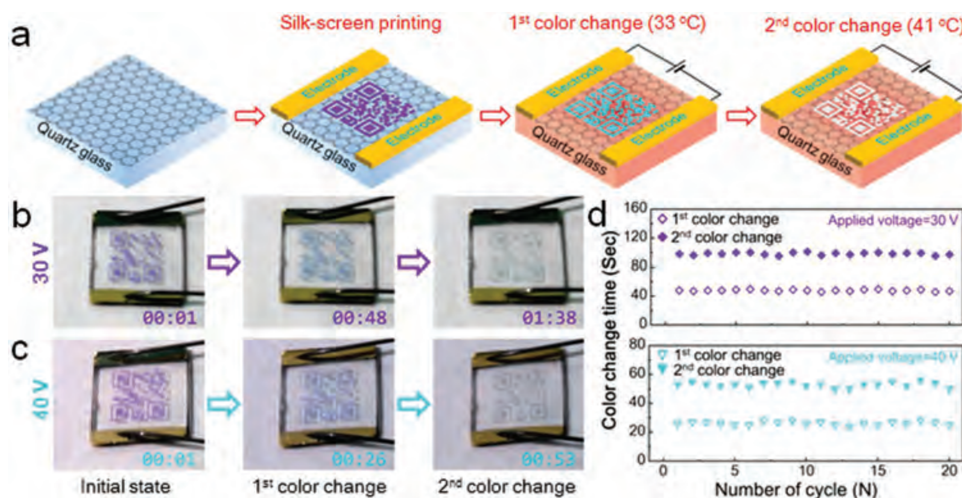

Figure 6. A heating device fabricated on graphene grown on quartz glass applied to thermochromic display. a) Schematic diagrams showing the operation of the graphene/quartz glass-based thermochromic display. b,c) Demonstration of the thermochromic display built on graphene/quartz glass at biases of 30 and 40 V. d) Cycling performance of the thermochromic display built on graphene/quartz glass at different input biases.

 © 2017 Wiley-VCH Verlag GmbH & Co. KGaA, Weinheim

optimizing the time and the temperature, the Ge evaporates completely during or immediately after formation of the monolayer graphene, thus resulting in the direct deposition of large-area and continuous graphene on dielectric substrates without metal contamination. The graphene synthesized on a transparent quartz glass is suitable for heating applications such as defogging and thermochromic displays. This promising technique for direct synthesis of graphene on dielectric substrates without metallic contamination may pave the way for the implementation of graphene for electronic and optoelectronic device application.

4. Experimental Section

Direct Growth of Graphene on Dielectric Substrates: DC magnetron sputtering (JGMF 500) was used to deposit 200-nm-thick Ge films on dielectric substrates (highly doped p-Si substrates with a 300-nm-thick thermal oxide layer, quartz glass, and sapphire). The samples were loaded in a tube furnace. After pumping down to 10^{-4} mbar, the pump was turned off and a mixture of hydrogen (23 sccm) and argon (230 sccm) was introduced until reaching atmospheric pressure. Without changing the gas flow rates, the samples were heated to 900–930 °C, which was close to the melting point of Ge. Graphene fabrication was carried out by adding methane (0.7 sccm) for 60–360 min. Afterward, the system was cooled to room temperature at a rate of 10 °C min^{-1}.

Transfer of Graphene: To characterize the quality and layer numbers of the graphene by TEM, it was necessary to transfer it to a copper grid. The TEM sample preparation was performed using a polymethylmethacrylate(PMMA)-assisted transfer method, as schematically shown in Figure S10 (Supporting Information). A thin film of PMMA was spin-coated onto the graphene/SiO_2/Si and baked at 100 °C for 10 min. It was immersed in a NaOH solution (100 mL and 10 wt%). Owing to the existence of PMMA, the sample floated on the surface of the solution. After immersing for 12 h, the silicon dioxide layer was completely etched by NaOH and the PMMA/graphene film was detached from the Si substrate while the Si substrate sank to the bottom of the solution. After the PMMA/graphene film was rinsed with deionized water several times, it was loaded onto a TEM copper grid and annealed at 100 °C for 10 min to improve adhesion. Finally, the PMMA was dissolved in hot acetone at 80 °C.

Characterization: The graphene/dielectric samples were characterized by Raman scattering (HORIBA Jobin Yvon HR800) using an Ar^+ laser with a wavelength of 514 nm and a spot size of 1 µm, SEM (Zeiss Gemini Ultra-55), X-ray photoelectron spectroscopy (XPS; PHI 5802, Physical Electronics Inc., Eden Prairie, MN), TEM (FET-Tecnai G2F20 S-7WIN), and atomic force microscopy (Bruker Multimode 8).

Electrical Measurements: The back-gated GFETs were fabricated with the graphene/SiO_2/Si. The source and drain electrodes (50-nm Au/10-nm Ti) were deposited by electron beam evaporation and a photolithographic step employing an inductively coupled plasma was used to pattern the graphene to form a field-effect transistor with a channel length of 8 µm and width of 2 µm. To improve the contact of the back-gated GFET device, annealing was performed in Ar (500 sccm) and H_2 (10 sccm) at 300 °C for 8 h in a tube furnace. The back-gated GFETs were characterized under ambient conditions using the Agilent (B1500A) semiconductor parameter analyzer. The mobility was extracted using the following equation:

$$\mu_{FET} = \frac{dI_{DS}}{dV_G} \cdot \frac{L}{W \cdot C_{ox} \cdot V_{DS}} \quad (1)$$

where L and W are the channel length and width, respectively, C_{ox} is the gate oxide capacitance (11 nF cm^{-2}), V_{DS} is the source drain voltage, I_{DS} is the source drain current, and V_G is the gate voltage. The linear regime of the transfer characteristics was used to obtain dI_{DS}/dV_G.

Supporting Information

Supporting Information is available from the Wiley Online Library or from the author.

Acknowledgements

Z.W. and Z.X. contributed equally to this work. The authors thank the Program of Shanghai Academic/Technology Research Leader (16XD1404200), the Key Research Project of Frontier Science, Chinese Academy of Sciences (QYZDB-SSW-JSC021), and the City University of Hong Kong Applied Research Grant (ARG) No. 9667122 for financial support. Partial support was also provided by the Center for Integrated Nanotechnologies (CINT), a US DOE nanoscience user facility jointly operated by Los Alamos and Sandia National Laboratories.

Conflict of Interest

The authors declare no conflict of interest.

[1] A. K. Geim, K. S. Novoselov, *Nat. Mater.* **2007**, *6*, 183.
[2] K. S. Novoselov, D. Jiang, F. Schedin, T. J. Booth, V. V. Khotkevich, S. V. Morozov, A. K. Geim, *Proc. Natl. Acad. Sci. USA* **2005**, *102*, 10451.
[3] J. Du, H.-M. Cheng, *Macromol. Chem. Phys.* **2012**, *213*, 1060.
[4] E. Yoo, J. Kim, E. Hosono, H.-S. Zhou, T. Kudo, I. Honma, *Nano Lett.* **2008**, *8*, 2277.
[5] T. Lin, I.-W. Chen, F. Liu, C. Yang, H. Bi, F. Xu, F. Huang, *Science* **2015**, *350*, 1508.
[6] S. Bae, H. Kim, Y. Lee, X. Xu, J.-S. Park, Y. Zheng, J. Balakrishnan, T. Lei, H. Ri Kim, Y. I. Song, Y.-J. Kim, K. S. Kim, B. Ozyilmaz, J.-H. Ahn, B. H. Hong, S. Iijima, *Nat. Nanotechnol.* **2010**, *5*, 574.
[7] L. Ju, B. Geng, J. Horng, C. Girit, M. Martin, Z. Hao, H. A. Bechtel, X. Liang, A. Zettl, Y. R. Shen, F. Wang, *Nat. Nanotechnol.* **2011**, *6*, 630.
[8] Y.-M. Lin, C. Dimitrakopoulos, K. A. Jenkins, D. B. Farmer, H.-Y. Chiu, A. Grill, P. Avouris, *Science* **2010**, *327*, 662.
[9] F. Schedin, A. K. Geim, S. V. Morozov, E. W. Hill, P. Blake, M. I. Katsnelson, K. S. Novoselov, *Nat. Mater.* **2007**, *6*, 652.
[10] Y. Ohno, K. Maehashi, Y. Yamashiro, K. Matsumoto, *Nano Lett.* **2009**, *9*, 3318.
[11] X. Li, X. Wang, L. Zhang, S. Lee, H. Dai, *Science* **2008**, *319*, 1229.

© 2017 Wiley-VCH Verlag GmbH & Co. KGaA, Weinheim

[12] X. Li, Y. Zhu, W. Cai, M. Borysiak, B. Han, D. Chen, R. D. Piner, L. Colombo, R. S. Ruoff, *Nano Lett.* **2009**, *9*, 4359.
[13] Y.-C. Lin, C. Jin, J.-C. Lee, S.-F. Jen, K. Suenaga, P.-W. Chiu, *ACS Nano* **2011**, *5*, 2362.
[14] Y.-C. Lin, C.-C. Lu, C.-H. Yeh, C. Jin, K. Suenaga, P.-W. Chiu, *Nano Lett.* **2012**, *12*, 414.
[15] A. Ismach, C. Druzgalski, S. Penwell, A. Schwartzberg, M. Zheng, A. Javey, J. Bokor, Y. Zhang, *Nano Lett.* **2010**, *10*, 1542.
[16] H.-J. Shin, W. M. Choi, S.-M. Yoon, G. H. Han, Y. S. Woo, E. S. Kim, S. J. Chae, X.-S. Li, A. Benayad, D. D. Loc, F. Gunes, Y. H. Lee, J.-Y. Choi, *Adv. Mater.* **2011**, *23*, 4392.
[17] J. Hofrichter, B. N. Szafranek, M. Otto, T. J. Echtermeyer, M. Baus, A. Majerus, V. Geringer, M. Ramsteiner, H. Kurz, *Nano Lett.* **2010**, *10*, 36.
[18] T. Kato, R. Hatakeyama, *ACS Nano* **2012**, *6*, 8508.
[19] Q.-Q. Zhuo, Q. Wang, Y.-P. Zhang, D. Zhang, Q.-L. Li, C.-H. Gao, Y.-Q. Sun, L. Ding, Q.-J. Sun, S.-D. Wang, J. Zhong, X.-H. Sun, S.-T. Lee, *ACS Nano* **2015**, *9*, 594.
[20] P.-Y. Teng, C.-C. Lu, K. Akiyama-Hasegawa, Y.-C. Lin, C.-H. Yeh, K. Suenaga, P.-W. Chiu, *Nano Lett.* **2012**, *12*, 1379.
[21] H. Kim, I. Song, C. Park, M. Son, M. Hong, Y. Kim, J. S. Kim, H.-J. Shin, J. Baik, H. C. Choi, *ACS Nano* **2013**, *7*, 6575.
[22] J. Hwang, M. Kim, D. Campbell, H. A. Alsalman, J. Y. Kwak, S. Shivaraman, A. R. Woll, A. K. Singh, R. G. Hennig, S. Gorantla, M. H. Rümmeli, M. G. Spencer, *ACS Nano* **2013**, *7*, 385.
[23] H. J. Song, M. Son, C. Park, H. Lim, M. P. Levendorf, A. W. Tsen, J. Park, H. C. Choi, *Nanoscale* **2012**, *4*, 3050.
[24] J. Chen, Y. Guo, Y. Wen, L. Huang, Y. Xue, D. Geng, B. Wu, B. Luo, G. Yu, Y. Liu, *Adv. Mater.* **2013**, *25*, 992.
[25] J. Chen, Y. Guo, L. Jiang, Z. Xu, L. Huang, Y. Xue, D. Geng, B. Wu, W. Hu, G. Yu, Y. Liu, *Adv. Mater.* **2014**, *26*, 1348.
[26] M. Son, H. Lim, M. Hong, H. C. Choi, *Nanoscale* **2011**, *3*, 3089.
[27] M. H. Rümmeli, A. Bachmatiuk, A. Scott, F. Börrnert, J. H. Warner, V. Hoffman, J.-H. Lin, G. Cuniberti, B. Büchner, *ACS Nano* **2010**, *4*, 4206.
[28] J. Sun, T. Gao, X. Song, Y. Zhao, Y. Lin, H. Wang, D. Ma, Y. Chen, W. Xiang, J. Wang, Y. Zhang, Z. Liu, *J. Am. Chem. Soc.* **2014**, *136*, 6574.
[29] J. Kwak, J. H. Chu, J.-K. Choi, S.-D. Park, H. Go, S. Y. Kim, K. Park, S.-D. Kim, Y.-W. Kim, E. Yoon, S. Kodambaka, S.-Y. Kwon, *Nat. Commun.* **2012**, *3*, 645.
[30] Q. F. Liu, Y. P. Gong, T. Wang, W. L. Chan, J. Wu, *Carbon* **2016**, *96*, 203.
[31] J. B. Pang, R. G. Mendes, P. S. Wrobel, M. D. Wlodarski, H. Q. Ta, L. Zhao, L. Giebeler, B. Trzebicka, T. Gemming, L. Fu, Z. F. Liu, J. Eckert, A. Bachmatiuk, M. H. Rummeli, *ACS Nano* **2017**, *11*, 1946.
[32] R. Muñoz, C. Munuera, J. I. Martínez, J. Azpeitia, C. Gómez-Aleixandre, M. García-Hernández, *2D Mater.* **2017**, *4*, 015009.
[33] H. K. Seo, K. Kim, S. Y. Min, Y. Lee, C. E. Park, R. Raj, T. W. Lee, *2D Mater.* **2017**, *4*, 024001.
[34] X. D. Chen, Z. L. Chen, W. S. Jiang, C. H. Zhang, J. Y. Sun, H. H. Wang, W. Xin, L. Lin, M. K. Priydarshi, H. Yang, Z. B. Liu, J. G. Tian, Y. Y. Zhang, Y. F. Zhang, Z. F. Liu, *Adv. Mater.* **2017**, *29*, 1603428.
[35] J. Sun, Y. Chen, M. K. Priydarshi, Z. Chen, A. Bachmatiuk, Z. Zou, Z. Chen, X. Song, Y. Gao, M. H. Rümmeli, Y. Zhang, Z. Liu, *Nano Lett.* **2015**, *15*, 5846.
[36] T. Ghani, M. Armstrong, C. Auth, M. Bost, P. Charvat, G. Glass, T. Hoffmann, K. Johnson, C. Kenyon, J. Klaus, B. McIntyre, K. Mistry, A. Murthy, J. Sandford, M. Silberstein, S. Sivakumar, P. Smith, K. Zawadzki, S. Thompson, M. Bohr, *IEDM Tech. Dig.* **2003**, *2003*, 978.
[37] C. Auth, C. Allen, A. Blattner, D. Bergstrom, M. Brazier, M. Bost, M. Buehler, V. Chikarmane, T. Ghani, T. Glassman, R. Grover, W. Han, D. Hanken, M. Hattendorf, P. Hentges, R. Heussner, J. Hicks, D. Ingerly, P. Jain, S. Jaloviar, R. James, D. Jones, J. Jopling, S. Joshi, C. Kenyon, H. Liu, R. McFadden, B. McIntyre, J. Neirynck, C. Parker, L. Pipes, I. Post, S. Pradhan, M. Prince, S. Ramey, T. Reynolds, J. Roesler, J. Sandford, J. Seiple, P. Smith, C. Thomas, D. Towner, T. Troeger, C. Weber, P. Yashar, K. Zawadzki, K. Mistry, *Symp. VLSI Tech. Dig.* **2012**, 131.
[38] G. Wang, M. Zhang, Y. Zhu, G. Ding, D. Jiang, Q. Guo, S. Liu, X. Xie, P. K. Chu, Z. Di, X. Wang, *Sci. Rep.* **2013**, *3*, 2465.
[39] A. C. Ferrari, D. M. Basko, *Nat. Nanotechnol.* **2013**, *8*, 235.
[40] X. Li, W. Cai, J. An, S. Kim, J. Nah, D. Yang, R. Piner, A. Velamakanni, I. Jung, E. Tutuc, S. K. Banerjee, L. Colombo, R. S. Ruoff, *Science* **2009**, *324*, 1312.
[41] R. R. Nair, P. Blake, A. N. Grigorenko, K. S. Novoselov, T. J. Booth, T. Stauber, N. M. R. Peres, A. K. Geim, *Science* **2008**, *320*, 1308.
[42] C.-Y. Su, A.-Y. Lu, C.-Y. Wu, Y.-T. Li, K.-K. Liu, W. Zhang, S.-Y. Lin, Z.-Y. Juang, Y.-L. Zhong, F.-R. Chen, L.-J. Li, *Nano Lett.* **2011**, *11*, 3612.

Received: March 21, 2017
Revised: April 12, 2017
Published online: May 31, 2017

© 2017 Wiley-VCH Verlag GmbH & Co. KGaA, Weinheim

Copyright WILEY-VCH Verlag GmbH & Co. KGaA, 69469 Weinheim, Germany, 2017.

Supporting Information

for *Small,* DOI: 10.1002/smll.201700929

Germanium-Assisted Direct Growth of Graphene on Arbitrary Dielectric Substrates for Heating Devices

Ziwen Wang, Zhongying Xue, Miao Zhang, Yongqiang Wang, Xiaoming Xie, Paul K. Chu, Peng Zhou, Zengfeng Di,* and Xi Wang*

Supplementary Information

Germanium-assisted Direct Growth of Graphene on Arbitrary Dielectric Substrates for Heating Devices

Ziwen Wang, Zhongying Xue, Miao Zhang, Yongqiang Wang, Xiaoming Xie, Paul K. Chu, Peng Zhou, Zengfeng Di,* and Xi Wang*

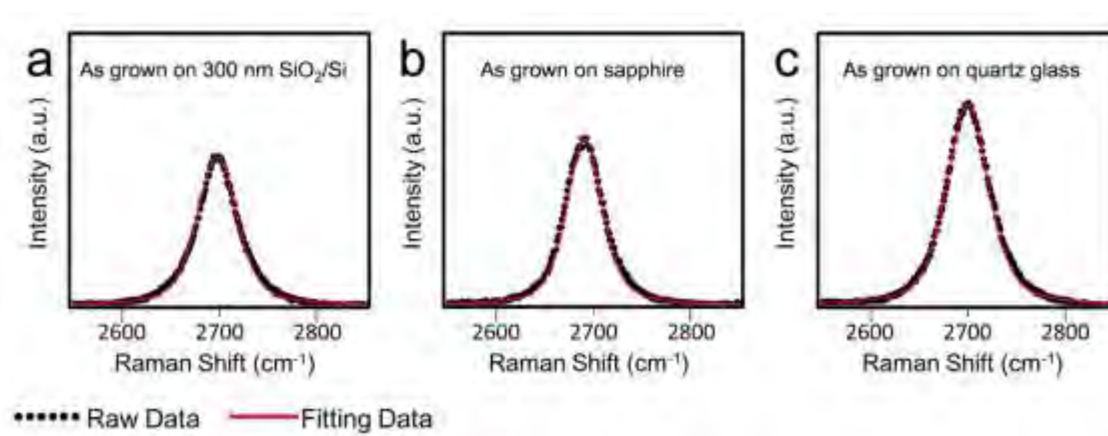

Figure S1. Raman 2D-peak Lorentzian fitting of the as-grown graphene on a) 300 nm SiO_2/Si, b) sapphire, and c) quartz glass. All the symmetric 2D peaks can be well fitted with a single Lorentzian curve, which proves that the as-synthesized graphene on a dielectric substrate is monolayered.

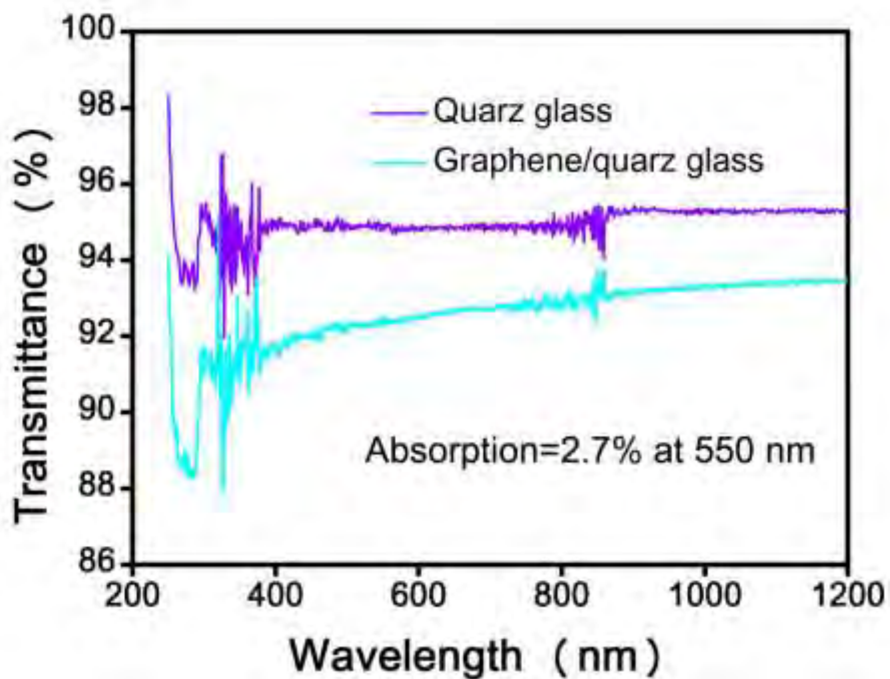

Figure S2. UV−vis transmittance spectra of quartz glass before and after graphene growth. At a wavelength of 550 nm, the graphene absorptivity is ~2.7%, which is consistent with the theoretical value of monolayer graphene.

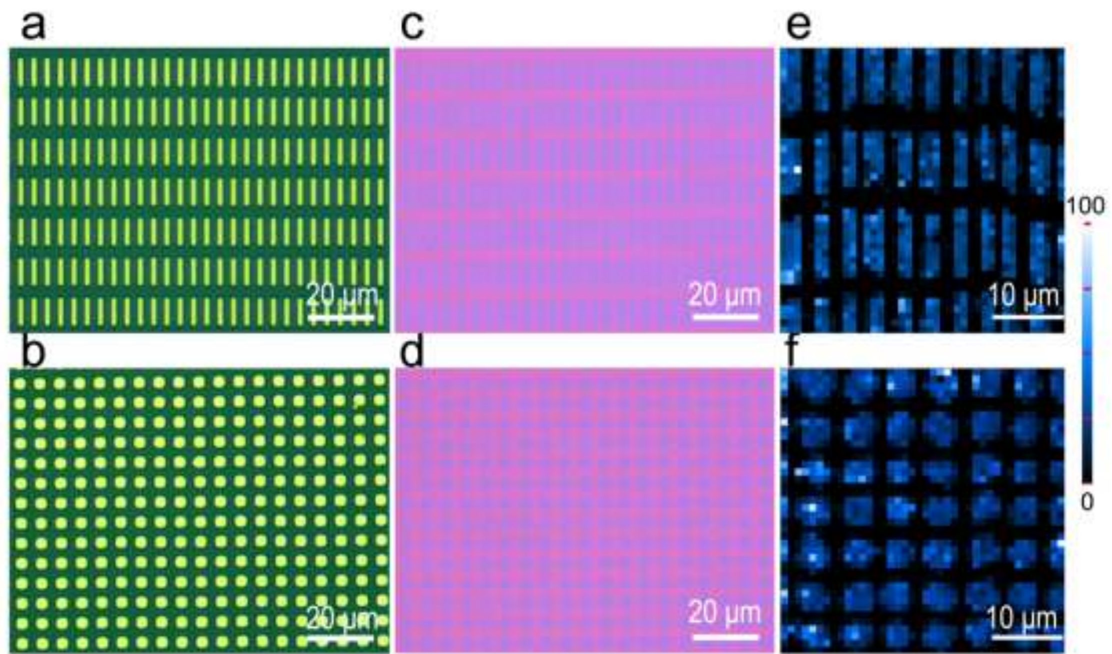

Figure S3. Various graphene patterns synthesized on 300 nm SiO_2/Si: a, b) Optical microscopy images of patterned Ge layer. c, d) Optical microscopy images of the corresponding as-grown graphene patterns. e, f) Raman intensity mapping for 2D-peak of graphene obtained in (c, d).

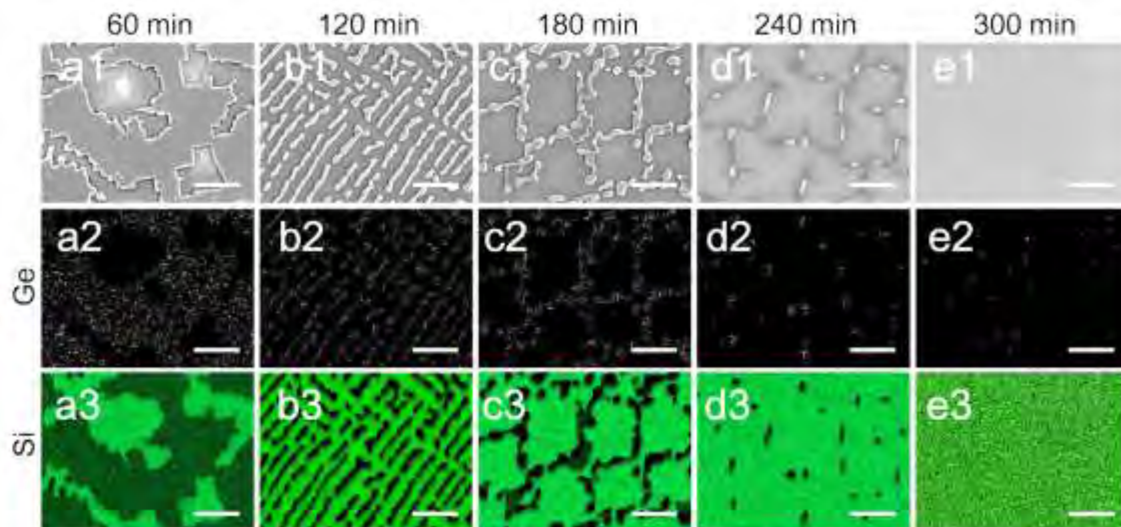

Figure S4. EDS maps of 200 nm Ge/300 nm SiO_2/Si samples after graphene growth at 920 ^{o}C for different duration: a1-e1) SEM images, a2-e2) EDS maps of Ge from the same area, a3-e3) EDS maps of Si from the same area. Scale bar: 20 μm.

Table S1. Germanium content deduced by EDS analysis of the 200 nm Ge/300 nm SiO_2/Si samples after graphene growth at 920 ^{o}C for different time.

Growth time (min)	60	120	180	240	300
Ge content (atomic %)	11.325	6.153	4.623	1.213	0.266

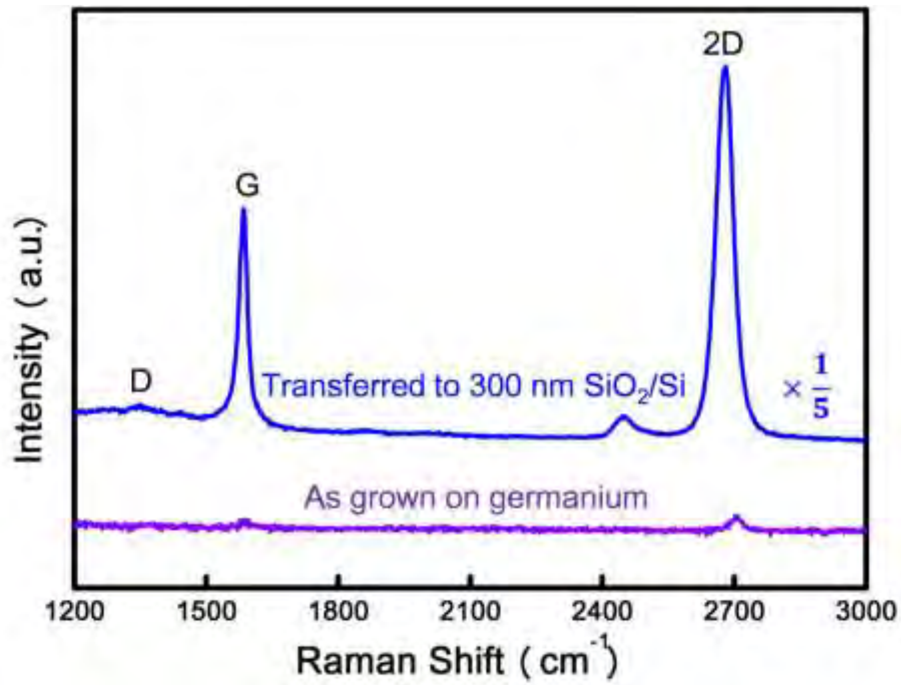

Figure S5. The comparison of Raman spectra obtained from graphene grown on bulk Ge and graphene transferred onto 300 nm SiO_2/Si. The intensity of graphene directly grown on bulk Ge is much lower than that of graphene transferred onto the SiO_2/Si substrate due to strong laser absorption and scattering by Ge substrate.

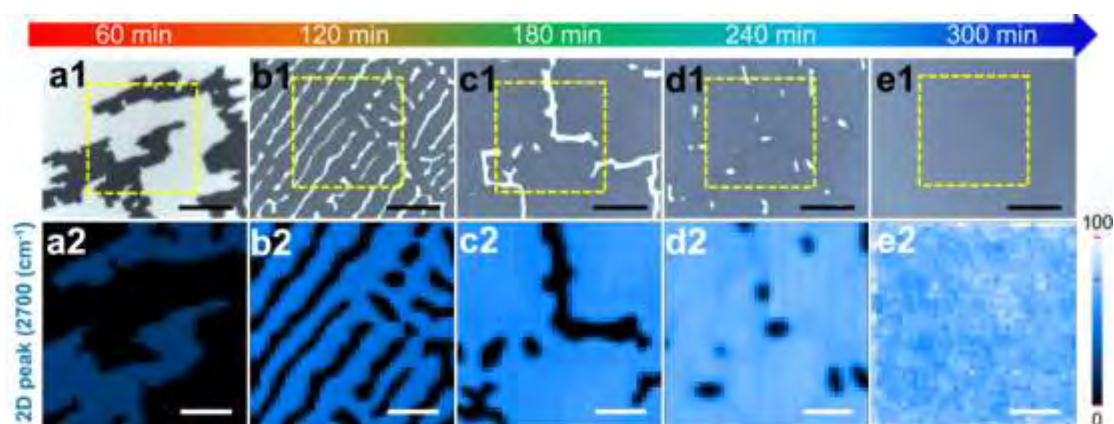

Figure S6. a1-e1), OM images of graphene grown on SiO_2/Si at 920 °C with different growth time. Scale bar: 20 μm. a2-e2), Raman mappings of the 2D peak of graphene from the selected areas marked by yellow dashed squares in a1-e1). Scale bar: 10 μm. Due to the strong absorption and scattering of excitation laser by the residual Ge, the scanning Raman image of the 2D band of graphene is closely related to the amount of residual Ge and thus makes a direct revelation of the distribution of graphene overlayer very difficult.

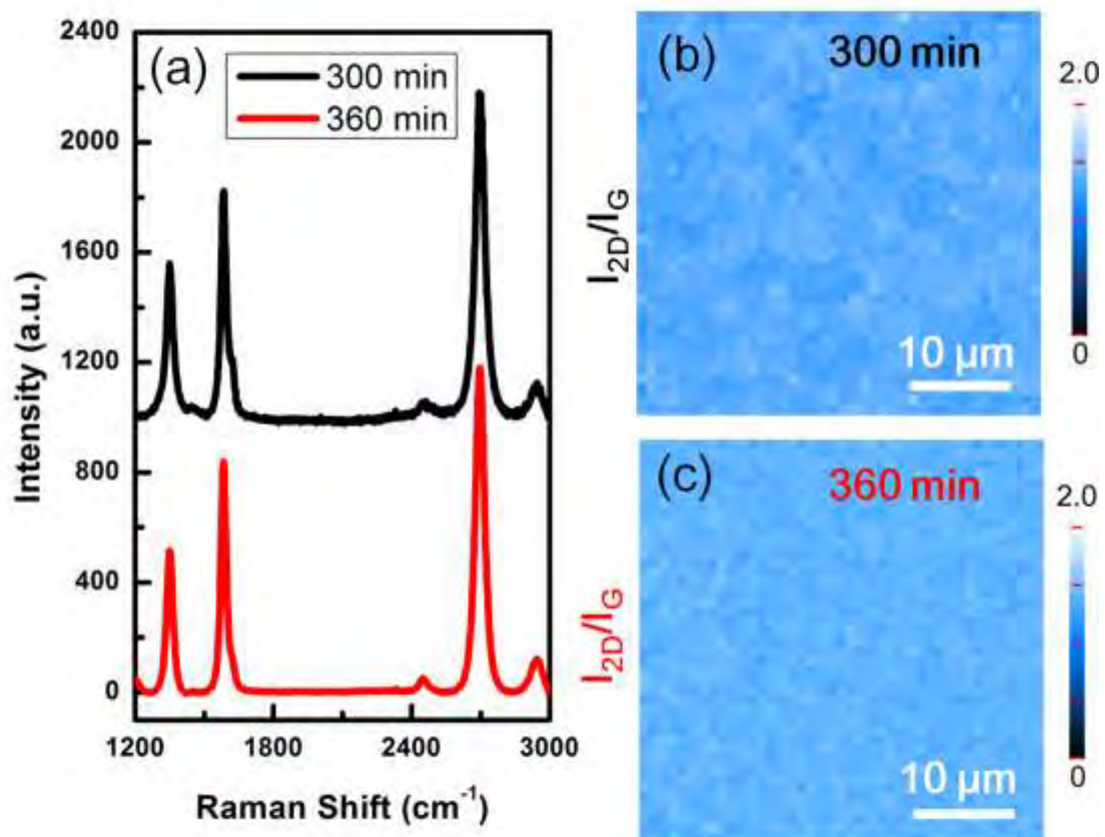

Figure S7 a) Raman spectra obtained from graphene grown on Ge coated SiO_2/Si for 300 and 360 minutes. b) Raman I_{2D}/I_G-mapping of graphene grown on Ge coated SiO_2/Si for 300 minutes. c) Raman I_{2D}/I_G-mapping of graphene grown on Ge coated SiO_2/Si for 360 minutes.

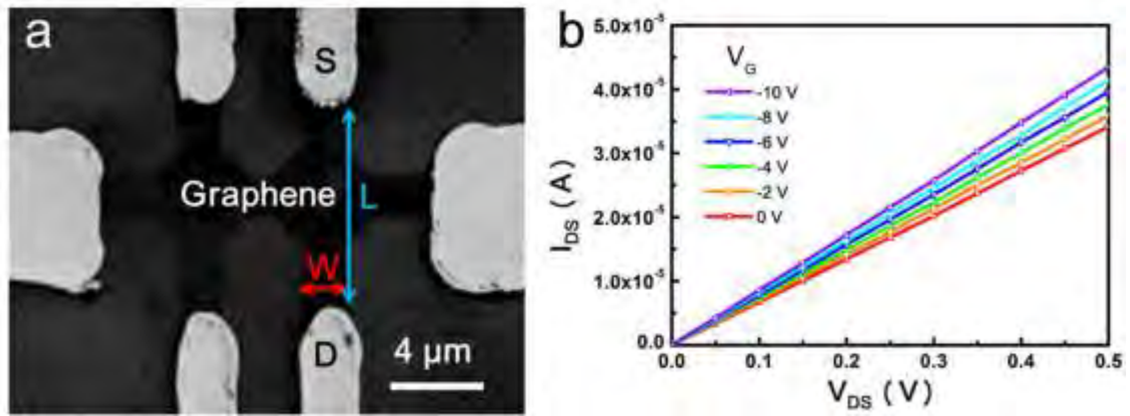

Figure S8. (a) SEM image of the fabricated GFET device. (b) Output characteristics (I_{DS}-V_{DS}) curves of graphene transistor at different V_G. The linear I_{DS}-V_{DS} curves indicate good ohmic contact between the Ti/Au electrodes and graphene channel.

Figure S9. Real-time defogging snapshots taken from the defogging video.

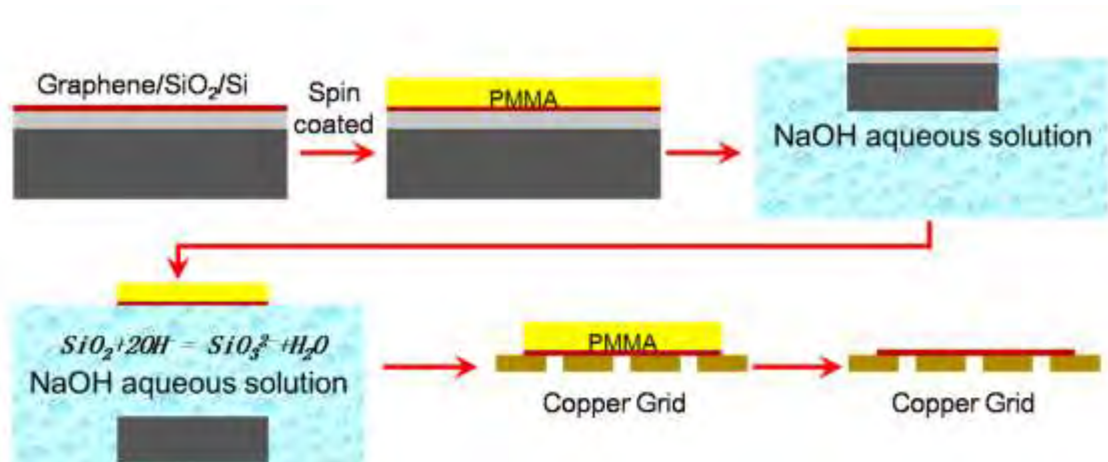

Figure S10. Schematic diagram of the graphene transfer process for TEM examination.